Journal of
Climatology & Weather Forecasting

Reda, J Climatol Weather Forecasting 2015, 3:3
DOI: 10.4172/2332-2594.1000138

Research Article Open Access

SMHI-RCA Model Captures the Spatial and Temporal Variability in Precipitation Anomalies over East Africa

Asmelash T. Reda*

Mekelle University, Mekelle Institute of Technology,Mekelle Tigray Ethiopia, Ethiopia

Abstract

This work assesses the performance of the Sweden's Meteorological and Hydrological Institute-the Rossby Centre Regional Atmospheric Climate Model, SMHI-RCA, in reproducing precipitation variability over Ethiopia. The simulated datasets, which are generated in the frame work of Coordinate Regional climate Downscaling Experiment (CORDEX) project, are validated by Global Precipitation Climatology Project (GPCP). Comparison of means, correlation coefficients, value of chi-square, bias test and test of significance showed that there is a good agreement between SMHI-RCA and GPCP rainfall at each grid point. Rotated Principal Components (RPCs) and the associated spectra for both datasets showed that the improvement of rainfall simulations is remarkable over different parts of the country. Classification using Hierarchical Clustering Analysis (HCLA) reasonably agrees with the reduction of data using Principal Component Analysis (PCA). Small scaled condensed homogeneous groups are identified from SMHI-RCA and GPCP datasets; several of them being shared by both. Zones of rainfall maxima for each cluster are primarily associated with the migration of Inter Tropical Convergence Zone (ITCZ); even though, elevation differences induce rainfall peaks to have a phase shift at local scale.

Keywords: Regional climate model; Rainfall; SMHI-RCA

Background

Ethiopia lies in the northeast part of Africa, north of the equator, covering a total area of 1,221,900 km^2. It's topography is composed of massive highlands along with complex mountains and dissected plateaus divided by Great Rift Valley running from northeast to southwest [1,2]. Elevation varies from a height at below sea level in the northeastern part of the country to higher than 3500 m above sea level in the northern highlands. Climate of Ethiopia is a typical of equatorial regions, but topography complicates its pattern and character [3-5]. It creates diverse microclimates ranging from hot deserts over the lowlands to cool, very wet over highlands [3,5,6].

Ethiopia's rainfall is highly variable both in amount and distribution across regions and seasons. There are regions that experience three seasons (bimodal type-1) with two rainfall peaks (where one peak is more prominent than the other) while some regions have four seasons with two similar rainfall peaks (bimodal type-2). There are still some regions which have two seasons with single rainfall peak (monomodal rainfall type) [7]. On the other hand, some areas have rainfall for 10 consecutive months; others receive rainfall for just a few months; while still others are characterized by three distinct rainfall seasons [2,3,7,8]. Mean annual rainfall distribution over the country is characterized by large spatial variations which range from about 2000 mm over some areas in the southwest to less than 250 mm over the Afar and Ogaden low lands [7].

The seasonal and annual rainfall variations are results of the macro-scale pressure systems and monsoon flows which are related to the changes in the pressure systems [7,9,10]. The most important weather systems that cause rain over Ethiopia include Sub-Tropical Jet (STJ), Inter Tropical Convergence Zone (ITCZ), Red Sea Convergence Zone (RSCZ), Tropical Easterly Jet (TEJ) and Somali Jet [7]. The spatial variation of the rainfall is, thus influenced by the changes in the intensity, position and direction of movement of these rain-producing systems over the country [11-13]. However, the fine scale spatial distribution of rainfall in Ethiopia is significantly influenced by topography. For example the detail spatial and temporal variability of rainfall along the Rift Valley show many abrupt changes and not well known yet [3,4].

So far, three identified seasons exist in Ethiopia. The first is the main rainy season from June to September, the second is the dry season from October to December/January, and the third is the small rainy season from February/March to May, known locally as Kiremt, Bega and Belg respectively. A brief description of the mechanisms for rainfall formation for each season is discussed below.

During Bega, most of the country is generally dry except the south and southeast of Ethiopia that receives its second important seasonal rainfall in this period. In this season, the country predominantly falls under the influence of warm and cool northeasterly winds. These dry air masses originate either from the Saharan anticyclone or from the ridge of high pressure extending into Arabia from the large high over central Asia (Siberia). Occasionally the northeasterly winds are interrupted when migratory low pressure systems originating in the Mediterranean area move southwards and interact with the tropical systems resulting into unseasonal rains over central and northern Ethiopia [7]. The development of the RSCZ also produces rains over northeastern coastal areas [14].

During Belg (the small rainy season), which is from March to May, coincides with the domination of the Arabian high as it moves towards the north Arabian Sea and the development of thermal low (cyclone) over the south Sudan. Winds from the Gulf of Aden and the Indian Ocean highs that are drawn towards this centre blow across central and southern Ethiopia [7,15]. These easterly and southeasterly moist winds produce the main rains in southern and southeastern Ethiopia and the Belg rains to the east-central part of the northwestern highlands.

***Corresponding author:** Asmelash T. Reda, Mekelle University, Mekelle Institute of Technology, Mekelle Tigray Ethiopia, Tel: +251914266715, E-mail: fasika20@gmail.com

Received July 27, 2015; **Accepted** August 14, 2015; **Published** August 27, 2015

Citation: Reda AT (2015) SMHI-RCA Model Captures the Spatial and Temporal Variability in Precipitation Anomalies over East Africa. J Climatol Weather Forecasting 3: 138. doi:10.4172/2332-2594.1000138

Citation: Reda AT (2015) SMHI-RCA Model Captures the Spatial and Temporal Variability in Precipitation Anomalies over East Africa. J Climatol Weather Forecasting 3: 138. doi:10.4172/2332-2594.1000138

Sometimes when the low-level westerly trough penetrates along the Rift Valley, the rainfall activity could linger for some days. The relationship between Ethiopian rainfall during Belg and the tropical cyclones over the southwest Indian Ocean indicates that low/high frequency of the cyclones resulted in excess/deficit rainfall [16]. There is also a meridional arm of the ITCZ due to the difference in heat capacity of the land surface and the Indian Ocean. This produces rainfall during February/March over southwest of Ethiopia [17]. The formation of intense and frequent tropical disturbances over the southeast Indian Ocean occurs simultaneously with Belg and Kiremt rainfall deficiency in Ethiopia [10].

During Kiremt the air flow is dominated by a zone of convergence in low-pressure systems accompanied by the oscillatory ITCZ extending from West Africa through the north of Ethiopia towards India. Major rain-producing systems during Kiremt are: the northward migration of the ITCZ; development and persistence of the Arabian and the Sudan thermal lows along 20°N latitude; development of quasi-permanent high-pressure systems over the south Atlantic and south Indian Oceans; development of the tropical easterly jet and its persistence and the generation of the low-level Somali jet which enhances low-level southwesterly flow. It is to be noted that Kiremt rainfall covers most of the country with the exception of the south and southeast of Ethiopia [3,7,8,13,17,18].

Data and Methodology

The SMHI-RCA simulated data, which are found from CORDEX downscaling experiment, are implemented for Ethiopia for the period 1996-2008. The model output, which is driven by ERA-interim runs, is validated by GPCP dataset [19,20]. Both datasets have horizontal resolution of 50 km. For analysis, the monthly averaged precipitation data and its anomalies are used for the period 1996 to 2008. Validation and inter-comparison are performed using comparison of means, mean error, correlation coefficients, bias test and test of significance. Model validation is begun by comparing model's mean precipitation with observations. Mean error calculates measure of dissimilarity. To see the model be consistent with GPCP in time at each grid point, we have utilized correlation, bais and T- tests. Clustering and classification of precipitation are done based on RPCA, spectral density and HCLA. RPCA is applied to determine dominant precipitation variability and uniform rainfall regions. Computation of periodicities and pseudo periodicities of RPCs are done using power spectral density. Finally, HCLA is used for further regrouping of precipitation in more localized scale [21].

Results and Discussion

Comparison of RCA and GPCP datasets

Mean: Figure 1 shows contour plots of mean precipitation over Ethiopia for the period October 1996 to December 2008. It reveals that RCA simulated rainfall is in a good agreement with GPCP observational rainfall at each grid point. Both datasets depict mean precipitation greater than 2.0 mm day^{-1} over the highlands but show relatively less rainfall lower than 2.0 mm day^{-1} over the rest part.

More sensitive measure of discrepancy can be obtained by subtracting GPCP from RCA at each grid point. Figure 2a shows distribution of differences of means. Model precipitation matches GPCP with some mixed positive and negative biases oscillating around zero in several parts of the country. Positive biases, with higher magnitude in the high altitudes, are seen over western part while along the Rift Valley, RCA appeared to be somehow underestimated by 1.0 mm day^{-1}.

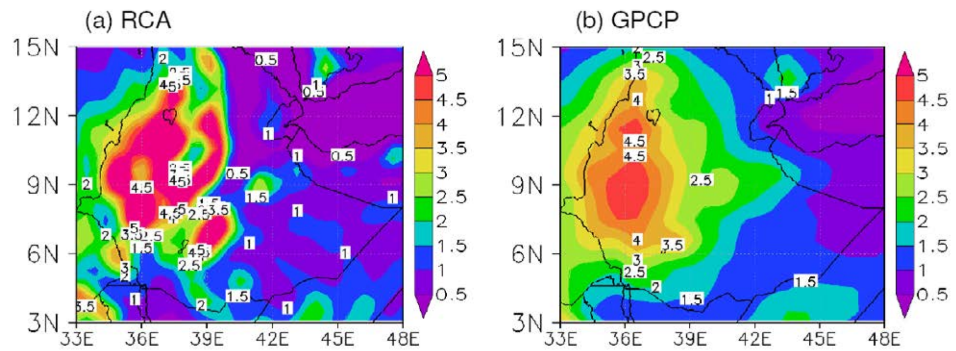

Figure 1: Mean precipitation in mm day^{-1}.

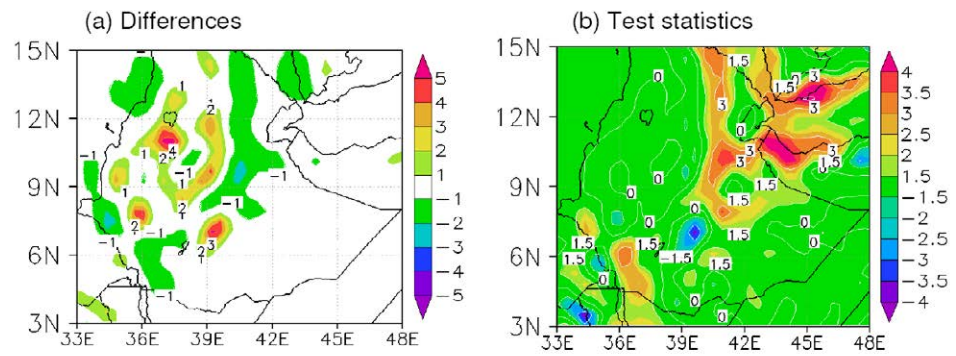

Figure 2: (a) Differences between RCA and GPCP. (b) Value of test statistics setting H_0: $\mu_{RCA}=\mu_{GPCP}$.

These observed differences might be due to lack of observational gauge dataset in these regions and/or due to efficient dynamic topographic adaptation behavior of RCA model over area where there is no gauge/less gauge density measurement within the grid box available.

It is important to see how the means estimate agree or disagree at each grid point. We have utilized the two-tailed T-test to calculate the frequency of agreement/disagreement between the two datasets at each grid point. To handle the temporal dependence at each location, effective number of degrees of freedom is computed from lag-1 autocorrelation coefficient as described by Janowiak and Wilks et al. [21,22]. This method is often reasonable approximations for representing the effective sample size. Critical values of Z for two tailed test are taken from Zwiers et al. [23]. Setting the null hypothesis 'mean of both datasets are equal at each grid point', Z value shows (Figure 2b), the differences are not significant at the level of 99% confidence interval (i.e. $Z<\pm 4$) over the entire region.

Bias test: Figure 3a shows model-simulated versus GPCP average precipitation datasets over Ethiopia from 1996 to 2008. RCA precipitation is in line with GPCP having apparent low partiality at two extreme points. RCA is somehow overestimated over the area that receives highest precipitation, but to some extent underestimated over the area that experiences lowest precipitation in spite of the existence of less number of disregarded outliers with large values. Evaluation of the model through difference versus grid points over the region (Figure 3b) supports this idea. Differences approximately equally distributed above and below the zero value lying mostly between ±2.0 mm day^{-1}.

Distribution of errors caused by differences between RCA and GPCP means are displayed in Figure 4. It is approximately Gaussian shaped having mean and variance respectively -0.264 and 0.820 delimited by maximum values ± 2.5 (Figure 4a). This shows 95% and 67% of all values of the differences lie in the interval of -0.264 ± 1.812 and -0.264 ± 0.906 respectively. Figure 4b strengthens this idea. Out of 980 grid points' values which are distributed in both directions from the mean, about 850 (90%) lie in the interval ± 1.5. Inside the interval ±0.5 mm, the number of positive difference in rainfall is identical to negative differences. However, outside this limit, negative differences are roughly twice as large as positive differences.

Correlation

For the time series assessment, Spearman's rank and Pearson correlation coefficients are calculated for RCA and GPCP monthly mean precipitation values at each grid point for the period 1996-2008. Spearman correlation (Figure 5a) shows RCA and GPCP are highly related by monotonic function with positive correlation coefficient (r>0.7) corresponding to simultaneous trend swing of them. Correlation is greater than 0.9 over all part of the region; however, in the northeast coast, near border areas and over the Red Sea, correlation is less but still higher than 0.7.

The better way to examine how the two datasets agree linearly is to look at Pearson correlation coefficient that requires linear relationship of variables. It is less sensitive than Spearman and only gave good value in the area where GPCP and RCA are related by linear function. From Figure 5b, high correlation and high linear relationship exist over the moorland located above the Rift Valley. Lowlands experience less precipitation and less correlation coefficient but still higher than 0.5. Pearson correlation coefficient fluctuates highly along the Rift valley which runs from northeast to southwest across Ethiopia. This can arise

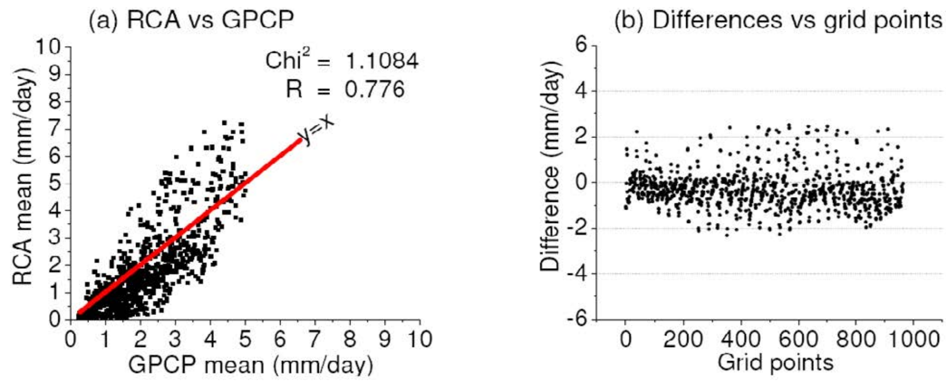

Figure 3: (a) RCA versus GPCP. (b) Precipitation differences between them versus grid points.

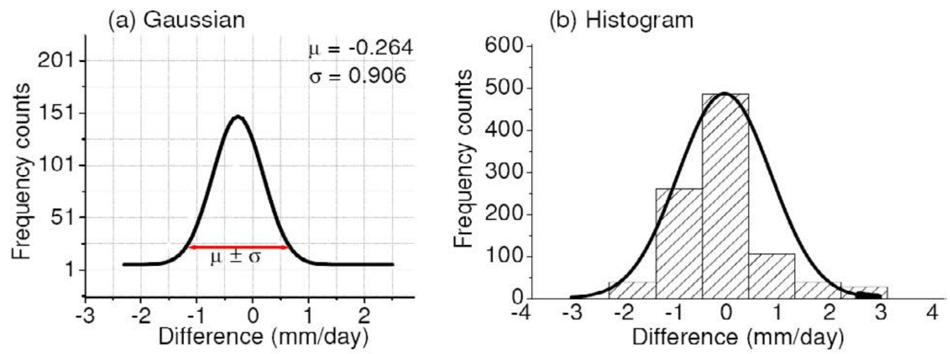

Figure 4: Frequency counts versus precipitation difference between RCA and GPCP.

Citation: Reda AT (2015) SMHI-RCA Model Captures the Spatial and Temporal Variability in Precipitation Anomalies over East Africa. J Climatol Weather Forecasting 3: 138. doi:10.4172/2332-2594.1000138

while the model adapts the complex orography during simulation. An area of low correlation (<0.5) is observed over the sea where gauge data are absent.

Test of significance has made for Pearson and Spearman correlation coefficients (Figure 6). It is calculated using a two-tailed T-test under the assumption 'there is no relationship between GPCP and RCA data (r=0)'. The effective number of degrees of freedom is calculated from first-order auto regressions following the method used by Zwiers et al. [23]. It is observed that Z lies above 7 for Spearman and above 5 for Pearson. Hence, the null hypothesis of 'no relationship in the paired population' totally rejected. There is significant relation between the two data in the whole domain.

Rotated empirical orthogonal functions, rotated principal components and spectral densities

To identify and compare dominant modes of rainfall variability, RPCA based on VARIMAX rotation method is used. It is applied to the monthly mean precipitation RCA and GPCP datasets. The leading four spatial patterns of REOFs and the corresponding scatter plots of RPC time series are displayed in Figures 7 and 8 respectively. Spectral

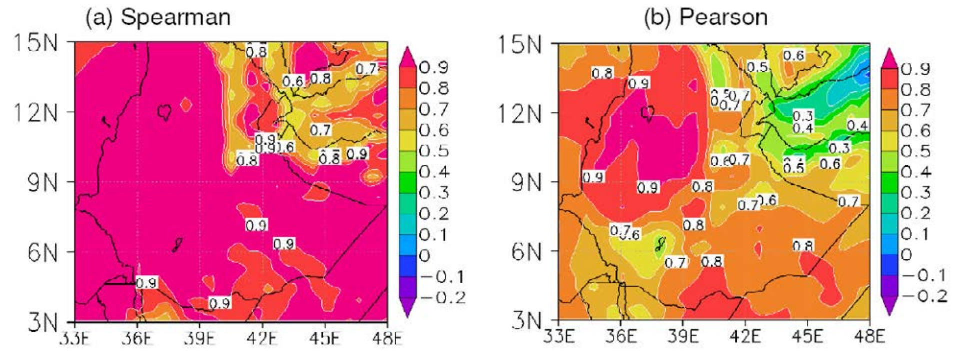

Figure 5: Correlation coefficient between RCA and GPCP.

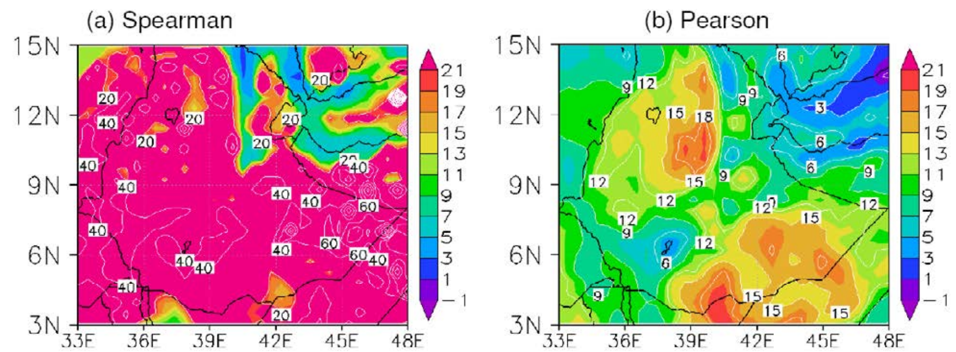

Figure 6: Value of test statistics setting H_0: r=0.

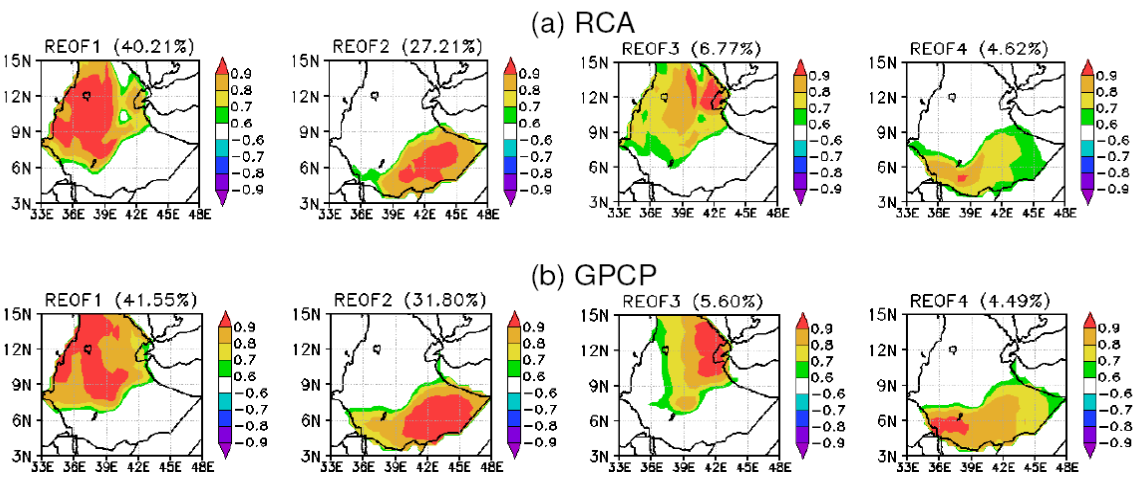

Figure 7: Correlation based leading four REOFs.

Citation: Reda AT (2015) SMHI-RCA Model Captures the Spatial and Temporal Variability in Precipitation Anomalies over East Africa. J Climatol Weather Forecasting 3: 138. doi:10.4172/2332-2594.1000138

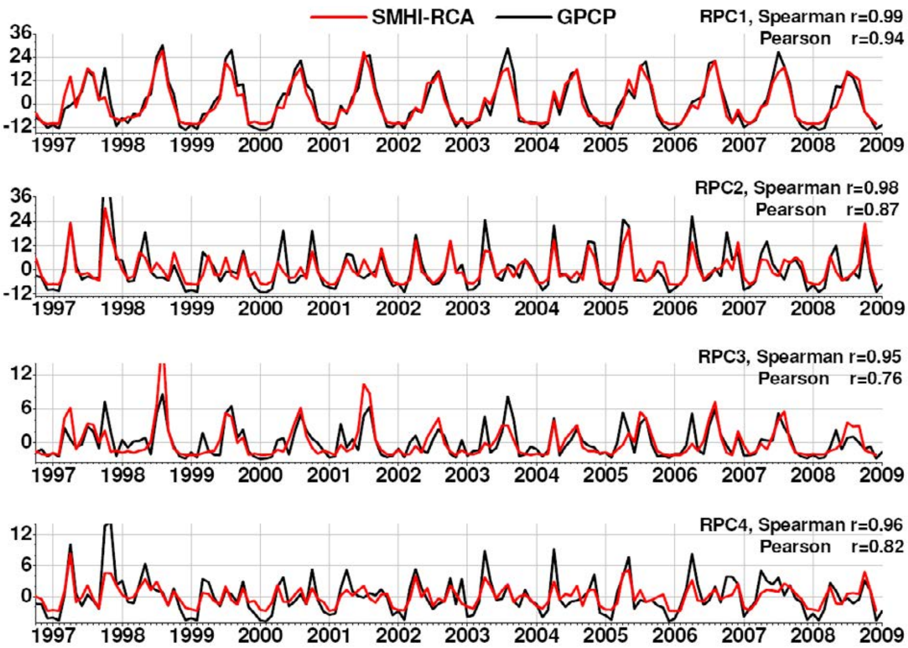

Figure 8: Scaled leading four RPCs and correlation values between RCA's and GPCP's RPCs.

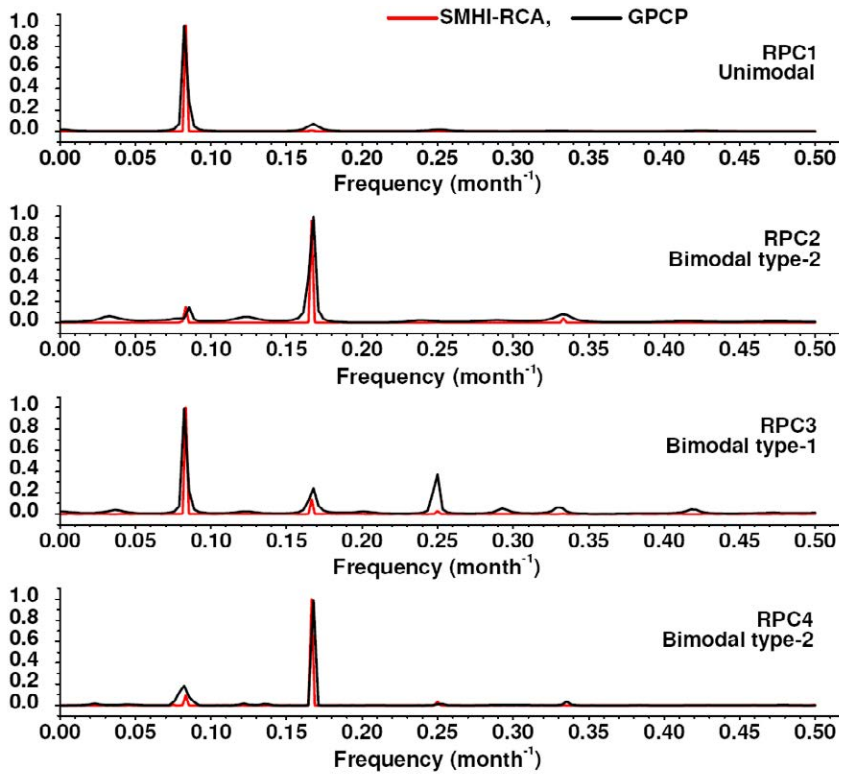

Figure 9: Normalized spectral density of the four leading RPCs for RCA and GPCP.

density associated with the autoregressive (AR) model was utilized to identify pseudo periodicities of the leading RPCs (Figure 9).

The results show the first four REOFs/RPCs account for 78.81% and 84.4% (respectively for RCA and GPCP) fraction of the total variance. They depict spatial and temporal pattern of homogeneous precipitation zones. Spectra of the RPCs exhibit dominant peaks at frequency f=0.167 month^{-1} (period T=6 months) and f=0.83 month^{-1} (T=12 months). Based on the spectral peaks, rainfall can be divided into unimodal (one season) and bimodal (two seasons) types. Bimodal is further splited up to bimodel type-1 and bimodal type-2.

REOF1 captures the well-known precipitation pattern exists in the north Ethiopia and have better correlated with northwestern and central highlands. This mode accounts for the largest amount of variance (40.21% and 41.55% for RCA and GPCP respectively). RPC1 time series, which is associated with REOF1, shows inter-seasonal variability. It has one dominant broad width associated with the long rainy season (JJAS) attaining maximum near July. Spectrum of RPC1 has strong signal at 12 months that corresponds to unimodal rainfall type (Kiremt season) [7].

REOF2 explains 27.21% and 31.8% (respectively for RCA and GPCP) fractions of the total variability. It involves rainfall anomalies over the southern Ethiopia and is strongly correlated with southeastern portion. Its spectrum has strong signal at 6 months and hence explains two seasons of roughly equal length and amplitude (bimodal type-2) peaking in October and April months. It has two distinct rainy periods (SON and MAM/Belg), separated by well-marked dry periods (DJF and JJA). Forward (northward movement) and retreat (southward movement) of ITCZ give rise to a bimodal rainfall pattern [3].

The spatial patterns of REOF3 appear to capture the east and northeastern precipitation pattern. It explains 6.77% and 5.6% (respectively for RCA and GPCP) of the total variance. Spectrum of RPC3 exhibits two unequal peaks that stand for bimodal type-1 mode. The two stronger peaks below one year suggest occurrence of two unequal precipitation patterns or existence of long (Kiremt) and short (Belg) rain seasons.

REOF4 explain only about 4.62% and 4.49% of the total variance for RCA and GPCP respectively. RPC2 and RPC4 signals, that have a periodicity of around 6 months, capture similar zone though RPC4 is more correlated with southwest and has better peak value in April than in October. The other unmentioned principal components capture the rest random variations departing from overall regional value.

These methods confirm the previous classification made by NMSA (1996). Monomodal rainfall pattern in the northern Ethiopia (June-September (Kiremt)) and bimodal rainfall pattern in southern Ethiopia (March-May (Belg) and September-November (SON). During Kiremt the air flow is dominated by a zone-of convergence in low-pressure systems accompanied by the oscillatory ITCZ extending from West Africa through the north of Ethiopia towards India. There is convergence between the air stream of African southwest monsoons diverted from the south Atlantic southeast trades and the Indian southwest monsoon on the Ethiopian highlands, especially on the western, central and eastern high grounds, resulting in heavy rainfall over the region [7]. Major rain-producing systems during Kiremt are: the northward migration of the ITCZ; development and persistence of the Arabian and the Sudan thermal lows; development of quasi-permanent high-pressure systems over the south Atlantic and south Indian Oceans; development of the tropical easterly jet and its persistence and the generation of the low-level Somali jet which enhances low-level southwesterly flow [17]. The Belg season coincides with the domination of the Arabian high as it moves towards the north Arabian Sea. It is the short and long rainy season for eastern and southern Ethiopia respectively [7,15]. Major systems during the Belg are: the domination of the Arabian high as it moves towards the north Arabian Sea and the development of thermal low (cyclone) over the south Sudan. Winds from the Gulf of Aden and the Indian Ocean highs that are drawn towards this centre blow across central and southern Ethiopia [1,7,15]. These easterly and southeasterly moist winds produce the main rains in southern and southeastern Ethiopia and the Belg rains to the east and central part of the northwestern highlands.

The value on the right top of each layer in Figure 8 describes Spearman and Pearson correlation coefficients between RCA and GPCP rainfall signals. For RPC1, both RCA and GPCP data are highly linearly correlated; whereas for RPC2, RPC3 and RPC4; RCA and GPCP are better nonlinearly correlated than linear.

Clusters

As the climate is rather complex, another broad classification of rainfall is found important to identify diffused homogeneous precipitation zones. Two criteria are used to divide the country into similar rainfall zones: identical peaks and minimum-distance clustering method. These criteria are applied to RCA and GPCP precipitation datasets. First, similar rainfall peaks above grid mean have been computed and categorized to get initial classes. Then clustering using simple-linkage criterion is applied for further regrouping within each class. Finally, clustered precipitation zones are assigned to the same color. Figure 10 shows homogeneous precipitation series lying within groups. Peaks above grid mean each cluster/zone possesses are displayed on top of the legend. Uppermost dominant color is assigned to the corresponding cluster name. Asterisk show significant peaks which might not be ignored.

In this way ten small scale distinct homogeneous zones are identified, nine being shared by both. Naming of zones is done in line with the previous works labeled as Zone- $A_1 – A_2$, Zone- $B_1 – B_3$ Zone- $C_1 – C_4$, Zone-D and Zone-E. Except zone-C and zone-E all have maxima that fall in the JJAS (Kiremt). Out of these, zone-A has additional peak in March/April associated with Belg. Zone-C and Zone-E (southern and southeastern parts) has two distinct maxima (in April/May and October/November). Terrain induced peak precipitation is observed for zone-D. Higher altitude has earlier climax month than lower altitude.

Peaks of rainfall primary follow forward and retreat of ITCZ when the low-pressure trough follows the sun's apparent movement in the northern hemisphere. The exact position of the ITCZ changes over the course of the year, migrating across the equator from its northern most position over northern Ethiopia in July and August to its southern most position over southern Kenya in January and February. However, the great terrain diversity in the country have induced rainfall pattern to have wide variations at local scale.

As soon as the ITCZ migrates northwards and enters south Ethiopia, zones start attain climax rainfall. The discussion below is synchronized with the movement of ITCZ. Zone-C and zone-E have rainfall crest in April/May. Zone-B_3 and zone-B_2 have maxima in June and July respectively. Zone-B_1 (north of zone-B_2) and zone-A (the lowland east of zone-B_2) have climax rainfall in August. Zone-E and zone-C have second maxima in October and October/November respectively connected to retreat of ITCZ back to the south. For zone-D (Arisi mountain), topography shows a considerable part in bringing rainfall. Higher altitude experiences earlier and higher monthly mean rainfall. In general, this and previous works have showed the intra-seasonal precipitation variation over Ethiopia is the result of large scale changes in macro-scale pressure systems and monsoon flows [9,10]. However, the fine scale spatial distribution of precipitation is significantly influenced by topography [4,7].

Zone-B_3 represents west highlands and experiences the longest rainy season of all zones. Major weather systems accompanied by high elevation play a considerable part in bringing rainfall throughout most of the year [17]. Winds carrying moisture fluxes from different directions forced up to these high grounds easily exhausted and cool to

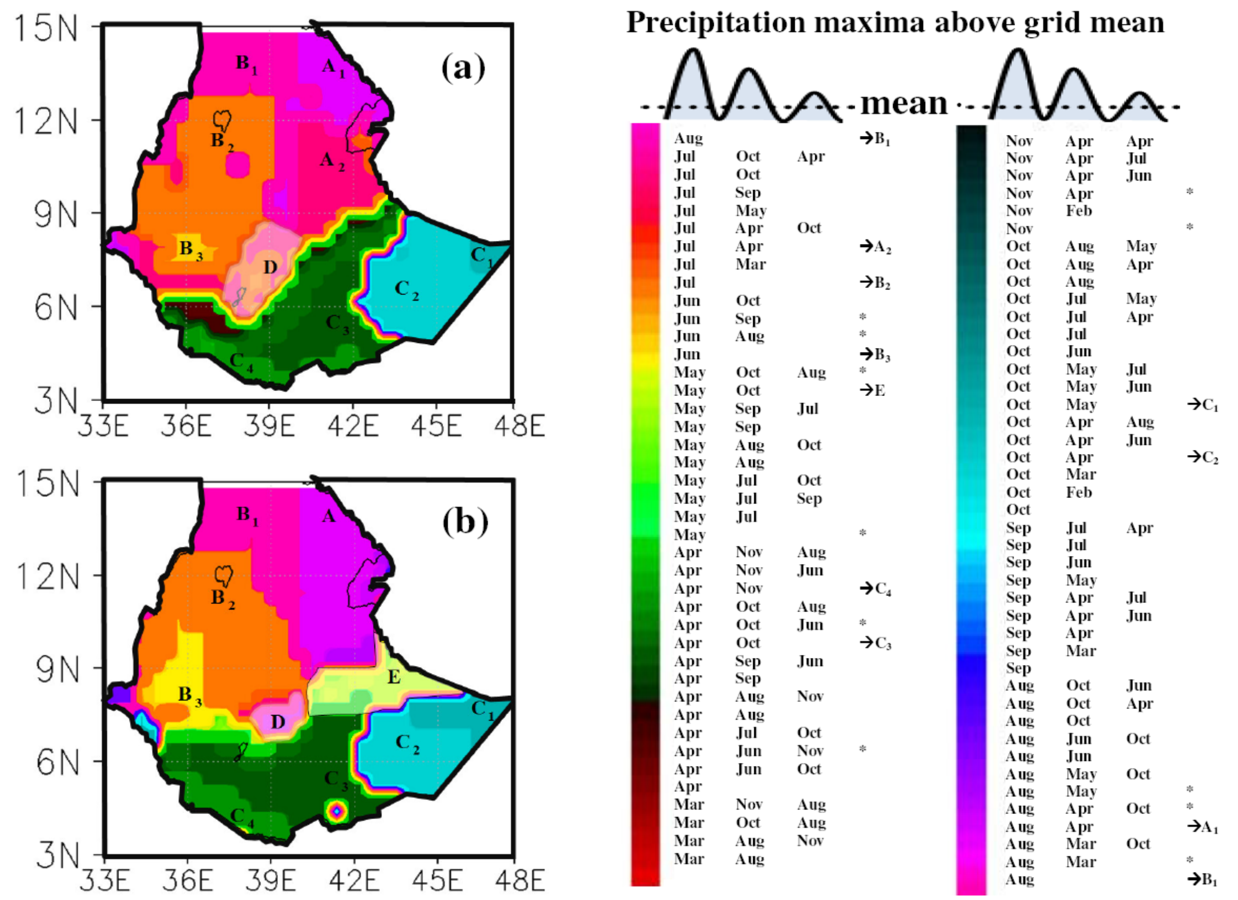

Figure 10: Contour map of merged clusters based on identical peaks and minimum-distance criteria: (a) RCA, and (b) GPCP.

give orographic rain [2]. Dominant peaks for zone-B_3 fluctuate between June and August. Zone-B_2 stands for the highlands found northwest of the Rift Valley and experiences heavy rainfall in Kiremt having climax in July. Elevation still affects this region. Zone-B_1 describes northern part of Ethiopia and has one dominant peak in August. The northeast lowland is captured by zone-A. It has two peaks in July and April (for Zone-A_2) or in August and March (for Zone-A_1) associated with Kiremt and Belg seasons (i.e. bimodal type-1). Zone-C represents bimodal type-2 with similar rainfall durations in MAM and SON having two dominant peaks in April/May and October/November. It describes precipitation series occurred over south and southeast. Well distinct four sub-groups (C_1-C_4) are found as a result of position of ITCZ, differences in elevation and wind velocity blowing over it. Zone-C_1 has highest peaks in October and May; zone-C_2 has peaks in October and April. Magnitudes of the two peaks are reversed for zone-C_3. Peaking in April than in October is because of the differences in the amount of moisture flux carried into and released over these zones by two winds. In April wind (with relatively higher moisture) from south Indian ocean crossing the flat lands of eastern Kenya [24,25]. Ellen et al. [2] starts to dominate the easterly/southeasterly wind associated with the Arabian Sea High Camberlin et al. [15] and brings more rainfall to zone-C_3 and zone-C_4. The southeastern part (zone-C_1 and zone-C_2) do not experience significant rainfall as the west part (zone-C_3 and zone-C_4) owing to: the development of low-level Somali Jet (also called East African low-level jet); simultaneous transition of low-level trade from southeast (ascending wind) to southwest (descending wind); consequently weakening of rainfall activity over these zones [26,27]. In JJAS, the Jet intensifies and enhances divergence and dryness over zone-C [24,25]. Clear distinction is observed aligned with 42°E due to splitting/deflecting of wind near Marsabit Mountain towards the two low pressure systems. One across southwestern Ethiopia that persist as Turkana Jet towards south Sudan and the other across southeastern Ethiopia, Indian Ocean to India [3,28,29]. In October month the Somali Jet starts to weaken and the associated wind having little/no deflection accompanied by enhanced orography effect and convective activity dominates over zone-C_1 and zone-C_2. On the contrary swelling of Turkana Jet weakens the convective activity over zone-C_3 and zone-C_4 [29]. Zone-C_4 (which is relatively lowland) has highest peak in April as zone-C_3 with the second peak shifted to November. On the other hand, rainfall over zone-E has bimodal type-2 feature with climaxes in May and October although RCA merges it with Zone-C. Navel of Ethiopia, which is identified by zone-D, is highly influenced by local elevation and hence by orographic rain. It has combined features just as zone-A and zone-B in both datasets. The pockets of matchless rainfall activity observed in both RCA and GPCP might be caused by the influence of local elevation on wind velocity and hence orographic rainfall [30]. In general, this and previous works confirm the large scale spatial variation of rainfall is influenced by the changes in intensity, position and direction of the rain-producing systems [11,12]. However, the small scale spatial distribution of rainfall in Ethiopia is significantly influenced by topography [4,7].

The results of hierarchical CLA more or less agree with the reduction of data using PCA. Zone-B is captured more by REOF1 to some extent by REOF3. It represents the distribution of precipitation over western, central and northern Ethiopia. Zone-A is more described by REOF3 and to some extent by REOF1. Zone-C is captured by both REOF2 and REOF4; likewise, the southeast and southwest parts are well explained by REOF2 and REOF4 respectively. Zone-D and Zone-E have intermediate characters and described by all REOFs.

Conclusion

This study examines the performance of the SMHI-RCA focusing on seasonal variations in precipitation over Ethiopia based on GPCP datasets. The basic statistical results showed that the model has good performance in simulating the precipitation variability and the spatial distribution of rain bands. However, it has been observed that RCA exhibits a little tendency to overestimate the highest rainfall over the highlands but underestimate the lowest rainfall over the eastern lowlands. RPCs and the associated spectra for both datasets demonstrate that the improvement of rainfall simulations is remarkable over the analysis domain. The leading four RPCs computed from PCA explain 37.55%, 26.84%, 10.30%, 3.16% and 41.55%, 31.8%, 5.6%, 4.49% for RCA and GPCP respectively. Spectra of the leading RPCs show dominant peaks at period of 6 months and 12 months that corresponds to unimodal (RPC1), quasi-bimodal (RPC3) and bimodal (RPC2 and RPC4) rainfall types. Classification using hierarchical clustering analysis (CLA) agrees with the reduction of data by PCA. Rainfall peaks at each zone primary follows the intensity, position and direction of the rain-producing systems; however, at the finer scale is significantly influenced by topography.

Acknowledgements

The authors would like to acknowledge for the data providers: KNMI Climate Explorer which is the primary web site for GPCP and other high resolution gridded observational datasets and Sweden's Meteorological and Hydrological Institute for making available RCA data on CORDEX data archive.

References

1. Yilma S, Zanke U (2004) Recent changes in Rainfall and Rainy Days in Ethiopia. International Journal of Climatology 24: 973-983.
2. Ellen V, Asgeir S (2011) Moisture transport into the Ethiopian highlands. International Journal of Climatology 10: 249-263.
3. Nicholson SE (1996) A review of climate dynamics and climate variability in eastern Africa. In: Johnson TC, Odada E (eds) The limnology, climatology and palaeoclimatology of the East African Lakes. Gordon and Breach, Amsterdam, pp. 25-56.
4. Slingo J, Spencer H, Hoskins BJ, Berrisford P, Black E (2005) The meteorology of the western Indian Ocean and the influence of the East African Highlands Philosophical Transactions of the Royal Society 363: 25-42.
5. Dinku T, Ceccato P, Grover-Kopec E, Lemma M, Connor SJ, et al. (2007) Validation of satellite rainfall products over East Africa's complex topography. International Journal of Remote Sensing 28: 1503-1526.
6. Segele ZT, Lamb PJ, Leslie LM (2009) Large-scale atmospheric circulation and global sea surface temperature associations with Horn of Africa June-September rainfall. International Journal of Climatology 29: 1075-1100.
7. National Meteorology Service Agency (1996) Climatic and agroclimatic resources of Ethiopia. National Meteorological Services Agency of Ethiopia. Meteorological Research Report Series 1: 1-137.
8. Korecha D, Barnston AG (2007) Predictability of June-September Rainfall in Ethiopia. Monthly Weather Review 135: 628-650.
9. Haile T (1987) A case study of seasonal forecasting in Ethiopia. WMO Regional Association I, Geneva pp 53-76.
10. Bekele F (1997) Ethiopian use of ENSO information in its seasonal forecasts. Internet J Afr 2: 2.
11. Tadesse T (1994) The influence of the Arabian Sea storms/depressions over the Ethiopian weather. Proc. Int. Conf. On Monsoon Variability and Prediction, WCRP-84 and WMO Tech. Doc. 619, World Meteorological Organization, Geneva, pp. 228-236.
12. Camberlin P (1995) June-September rainfall in northeastern Africa and atmospheric signals over the tropics: a zonal perspective. International Journal of Climatology 15: 773-783.
13. Camberlin P (1997) Rainfall anomalies in the source region of the Nile and their connection with the Indian summer monsoon. J Climate 10: 1380-1392.
14. Pedgley DE (1966) The Red Sea Convergence Zone. Weather 21: 394-406.
15. Camberlin P, Philippon N (2002) The East African March-May Rainy season: Associated Atmospheric dynamics and predictability over the 1968-1997 periods. J Climate 15: 1002-1019.
16. Shanko D, Camberlin P (1998) The Effect of the Southwest Indian Ocean Tropical Cyclones on Ethiopian Drought. International Journal of Climatology 18: 1373-1388.
17. Kassahun B (1987) Weather systems over Ethiopia. Proc. First Tech. Conf. on Meteorological Research in Eastern and Southern Africa, Nairobi, Kenya, UCAR: 53-57.
18. Segele ZT, Lamb PJ (2005) Characterization and variability of Kiremt rainy season over Ethiopia. Meteorology and Atmospheric Physics 89: 153-180.
19. Adler RF, Huffman GJ, Chang A, Ferraro R, Xie P, et al. (2003) The Version 2 Global Precipitation Climatology Project (GPCP) Monthly Precipitation Analysis (1979-Present). J Hydrometeor 4: 1147-1167.
20. Huffman GJ, Adler RF, Morrissey M, Bolvin DT, Curtis S, et al. (2001) Global Precipitation at One-Degree Daily Resolution from Multi-Satellite Observations. J Hydrometeor 2: 36-50.
21. Wilks DS (2006) Statistical Methods in the Atmospheric Sciences. (2ndedn) Academic, Amsterdam.
22. Janowiak JE, Gruber A, Kondragunta CR, Livezey RE, Huffman GJ (1998) A comparison of the NCEP–NCAR reanalysis precipitation and the GPCP rain gauge–satellite combined dataset with observational error considerations. J Climate 11: 2960-2979.
23. Zwiers FW and Von Storch H (1995) Taking Serial Correlation into Account in Tests of the Means. Journal of climate 8: 336-350.
24. Findlater J (1969) A major low-level air current near the Indian Ocean during the northern summer. Quarterly Journal of the Royal Meteorological Society 95: 362-380.
25. Findlater J (1977) Observational aspects of the low-level cross equatorial jet stream of the western Indian Ocean. Pure and Applied Geophysics 115: 1251-1262.
26. Flohn H (1965) Studies on the Meteorology of Tropical Africa. Bonner Meteorologische Abhandlungen 5: 57.
27. Flohn H (1987) Rainfall teleconnections in northern and northeastern Africa. Theoretical and Applied Climatology 38: 191-197.
28. Kinuthia JH, Asnani GC (1982) A Newly Found Jet in North Kenya (Turkana Channel). Monthly Weather Review 110: 1722-1728.
29. Kinuthia JH (1992) Horizontal and Vertical Structure of the Lake Turkana Jet. Journal of Applied Meteorology 31: 1248-1274.
30. Barbro J, Deliang C (2003) The influence of wind and topography on precipitation distribution in Sweden: statistical analysis and modelling. International Journal of Climatology 23: 1523-1535.

Citation: Reda AT (2015) SMHI-RCA Model Captures the Spatial and Temporal Variability in Precipitation Anomalies over East Africa. J Climatol Weather Forecasting 3: 138. doi:10.4172/2332-2594.1000138